

Volcanic impact on the Atlantic Ocean over the last millennium

J. Mignot¹, M. Khodri¹, C. Frankignoul¹, and J. Servonnat²

¹LOCEAN-IPSL UMR 7159 CNRS-IRD MNHN-UPMC, Case 100, Université Pierre et Marie Curie, 4 place Jussieu, 75252 Paris Cedex 05, France

²LSCE-IPSL UMR 8212, CEA-Orme des Merisiers, 91191 Gif-sur-Yvette Cedex, France

Received: 19 July 2011 – Published in Clim. Past Discuss.: 2 August 2011

Revised: 4 November 2011 – Accepted: 22 November 2011 – Published: 21 December 2011

Abstract. The oceanic response to volcanic eruptions over the last 1000 years is investigated with a focus on the North Atlantic Ocean, using a fully coupled AOGCM forced by a realistic time series of volcanic eruptions, total solar irradiance (TSI) and atmospheric greenhouse gases concentration. The model simulates little response to TSI variations but a strong and long-lasting thermal and dynamical oceanic adjustment to volcanic forcing, which is shown to be a function of the time period of the volcanic eruptions. The thermal response consists of a fast tropical cooling due to the radiative forcing by the volcanic eruptions, followed by a penetration of this cooling in the subtropical ocean interior one to five years after the eruption, and propagation of the anomalies toward the high latitudes. The oceanic circulation first adjusts rapidly to low latitude anomalous wind stress induced by the strong cooling. The Atlantic Meridional Overturning Circulation (AMOC) shows a significant intensification 5 to 10 years after the eruptions of the period post-1400 A.D., in response to anomalous atmospheric momentum forcing, and a slight weakening in the following decade. In response to the stronger eruptions occurring between 1100 and 1300, the AMOC shows no intensification and a stronger reduction after 10 years. This study thus stresses the diversity of AMOC response to volcanic eruptions in climate models and discusses possible explanations.

investigating natural and forced variations, as climate reconstructions are reaching a relatively high temporal resolution (Jones et al. 2001, Mann et al. 2009), and show substantial decadal to multidecadal fluctuations (e.g. Gray et al. 2004). However, reliable oceanic reconstructions are still very rare (Sicre et al. 2008, Masse et al. 2008, Richter et al. 2009), mainly because of the difficulty to obtain undisturbed high sedimentation rate and well-dated marine sediments. Meanwhile, computer resources are increasing so that climate integrations using state-of-the-art coupled ocean-atmospheric general circulation models (OAGCM) are becoming routinely available over this period, allowing investigations of the mechanisms of low frequency climate variability.

Several observational studies have shown that the ocean, and in particular the North Atlantic, plays a large role in decadal climate variability (e.g. Knight et al., 2005 Sutton and Hodson 2003, 2005). The relative importance of the various external forcings, however, remains debated. In model studies, this is partly due to their different representation and partly to divergent model responses. The researchers van der Schrier et al. (2002) and Hofer et al. (2010) suggested that external forcings, primarily variations of the total solar irradiance (TSI), act as modulators of the natural climate variability. Goosse and Renssen (2006) reported a decrease of the large scale Atlantic Meridional Overturning Circulation (AMOC) for increasing TSI, similar to the response to an increased atmospheric CO₂ concentration. In Zorita et al. (2004), on the contrary, the TSI does not have a significant impact on the AMOC.

Volcanic eruptions constitute another important external forcing over the last millennium. Their climatic impact has been largely investigated in terms of atmospheric thermal and dynamical anomalies in relation with the North Atlantic Oscillation, the El Niño-Southern Oscillation or the monsoons systems (e.g. Oman 2006, Shindell et al. 2004, Stenchikov et al. 2006, Trenberth and Dai 2007). Probably because of the lack of reliable reconstructions, fewer studies have

1 Introduction

Understanding the climate fluctuations at decadal timescales and the climate response to external forcing is of prime importance to anticipate and understand future climate changes. The last millennium constitutes an interesting framework for



Correspondence to: J. Mignot
(juliette.mignot@locean-ipsl.upmc.fr)

focused on their effect on the oceans. Church et al. (2005) and Gleckler et al. (2006) suggested that oceanic anomalies following a volcanic eruption could last more than a decade. Applying sensitivity response studies to relatively recent eruptions (the Pinatubo in 1991 and the Tambora in 1815), Stenchikov et al. (2009) showed that, while radiative forcing produced by these explosive events lasted for about 3 years, the volcanically induced tropospheric temperature anomalies remained significant for seven years, the sea ice responded on decadal time scales, and the deep ocean temperature, sea level, salinity and the AMOC were perturbed for several decades to a century. In particular, the AMOC strengthened by roughly 10%, but the amplitude to the response scaled less than linearly with the strength of the eruption. In response to a super-eruption with 100 times the Pinatubo amount of sulphuric acid released in the stratosphere, Jones et al. (2005) found that the AMOC doubled in intensity after nine years. Ottera et al. (2010), Ortega et al. (2011) and Zanchettin et al. (2011) all found an intensification of the AMOC in long simulations forced by both reconstructions of volcanic eruptions and variations in TSI. This response was associated to a persistent positive phase of the North Atlantic Oscillation (NAO) in Ottera et al. (2010). In both Ortega et al. (2011) and Zanchettin et al. (2011) (2011), the AMOC intensification is induced by enhanced convection in the Nordic Seas rather than in the Labrador Sea as in Ottera et al. (2010).

Several studies have also begun to point out the specificity of the thirteenth century in terms of intense volcanic activity and the possibility for a cumulative impact on the ocean (e.g. Zhong et al. 2010). The second half of the thirteen century is indeed the most perturbed half century of the past 1500 years (Jansen et al. 2007). In two out of four simulations, Zhong et al. (2010) found a centennial-scale climate change following the succession of decadal paced eruptions following the 1257–1258 mega-eruption. They highlighted a coupled ice-ocean interaction between the subpolar North Atlantic, a reduced extension of the AMOC into the northern North Atlantic, and the Arctic Ocean, which maintained significantly expanded sea ice and reduced surface air temperatures for at least 100 years. However, the feedback mechanism depended on other factors since it was only activated in half of the simulations. In this context, it is important to highlight that while both Stenchikov et al. (2009) and Ottera et al. (2010) found a significant intensification of the AMOC following volcanic eruptions, the first study was based on sensitivity experiments following single eruptions of different intensities and the other based on composite analysis over the last 600 years of the millennium, thereby excluding the particular succession of events of the thirteenth century.

Here, we explore the interannual to decadal oceanic response to volcanic activity in a coupled OAGCM forced by a full set of reconstructed external forcings over the last millennium. Sicre et al. (2011) have shown that the simulated

sea surface temperature (SST) in the northern North Atlantic compares well with a recent high resolution SST reconstruction off Iceland. We propose to describe more thoroughly the oceanic response to the major volcanic eruptions of the last millennium and investigate the mechanisms for the oceanic circulation adjustment. The model configuration and the forcings are presented in Sect. 2. The oceanic response to solar and volcanic forcing are compared in Sect. 3 and the temperature response to volcanic eruptions is discussed in Sect. 4. In Sect. 5, we investigate the response of the Atlantic circulation to isolated volcanic eruptions (occurring after year 1400) and in Sect. 6, we highlight the differences with the twelfth and thirteenth century. Conclusions are given in Sect. 7.

2 Model and experiment

2.1 The coupled model

We use the IPSLCM4 v2 climate model developed at the Institut Pierre-Simon Laplace (Marti et al. 2010). This model couples the LMDz4 atmosphere GCM (Hourdin et al. 2006) and the ORCHIDEE 1.9.1 module for continental surfaces (Krinner et al., 2005) to the OPA8.2 ocean model (Madec et al. 1998) and the LIM2 sea-ice model (Fichefet and Maqueda 1997), using the OASIS coupler (Valcke et al. 2000). The resolution in the atmosphere is 3.75° in longitude, 2.5° in latitude, and 19 vertical levels. The ocean and sea-ice are implemented on the ORCA2 grid (averaged horizontal resolution $2 \times 2^\circ$, refined to 0.5° around the equator, 31 vertical levels). In all simulations, the vegetation was set to a modern climatology from Myneni et al. (1997). After a 310 year spin up with preindustrial greenhouse gases (GHG) concentrations and tropospheric aerosols, two simulations were run. The first one is a 1000-year control simulation with the same preindustrial conditions as the spin up, also used in Servonnat et al. (2010). The main characteristics of the AMOC in the model and its sensitivity to freshwater have been discussed by Swingedouw et al. (2007). They showed that an excess of freshwater flux over the Labrador Sea was responsible for the lack of deep convection in this region and the relatively weak AMOC (11 Sv) in the model. Deep convection in the northern North Atlantic only takes place in the Nordic Seas and south of Iceland (Marti et al. 2010). The natural variability of the AMOC, its link to deep convection and its impact on the atmosphere have been studied by Msadek and Frankignoul (2009). They showed that the multidecadal fluctuations of the AMOC are mostly driven by the deep convection in the subpolar gyre with a time lag of 6 to 7 years. Convection in the subpolar gyre is itself primarily influenced by anomalous salinity advection caused by the variability of the East Atlantic Pattern (EAP), second dominant mode of atmospheric variability in the North Atlantic region. The lack of Labrador Sea convection in the model probably

explains the dominance of the EAP (as opposed to the North Atlantic Oscillation) in forcing multidecadal variations of the AMOC. The second simulation (LM2SV) was forced with a reconstruction of TSI, GHGs concentrations, changes in orbital parameters, and radiative effect of volcanic eruptions over the last millennium, from 850 to 2000 A.D. The choice and implementation of the forcings are discussed below. To reduce the influence of the model drift, a quadratic trend was removed from each variable and grid point.

As our main focus is on the oceanic response to volcanic eruptions at interannual to decadal timescales, all data are considered in annual mean, or seasonal mean for such variables as sea ice cover and mixed layer depth.

2.2 External forcing over the last millennium

A number of different reconstructions for TSI variations have been produced (e.g. Jansen et al. 2007), mostly differing in the estimated reduction of total irradiance during the 17th century Maunder Minimum, which ranges from 0.08 % to 0.65 % (1.1 to 8.9 W m^{-2}) of the contemporary value. Ammann et al. (2007) found that a TSI decrease of about 0.25 % during the Maunder Minimum produces a realistic amplitude of the Northern Hemisphere temperature change in climate models. However, recent progress in solar physics (Foukal et al. 2004, Solanki and Krivova 2006, Gray et al. 2010) imply that the TSI variations between the Maunder Minimum and present day value are about 0.1 %. On the other hand, even more recently, Shapiro et al. (2011) found indications of very large variations of the solar forcing during the Holocene. Nevertheless, as the weak scaling is recommended for the third phase of the paleoclimate modeling inter-comparison project (PMIP III, Schmidt et al. 2011), we use the TSI reconstruction by Vieira and Solanki (2010) and Krivova et al., (personal communication, 2009), which follows it. The corresponding variations of the raw shortwave input at the top of the atmosphere is shown in Fig. (2) (top panel).

Large volcanic eruptions inject sulfur gases into the stratosphere, which convert to sulfate aerosols with a residence time of about a year. The aerosol cloud has several effects on radiative processes, most notably by backscattering part of the incoming solar radiation, which induces a net cooling at the Earth's surface (e.g. Robock 2000). Thus, until recent years, most modelling groups (e.g. Jansen et al. 2007) have represented the volcanic forcing by altering the solar constant. Although such a coarse approach leads to hemispheric averages that compared reasonably well to a "blend" of proxy and/or instrumental reconstructions (e.g. Goosse et al. 2005, Stendel et al. 2006), it does not properly represent regional and seasonal variations. It is indeed known that the climatic impact of volcanic eruptions highly depends on the season, and that latitudinal dependence of the cooling in the troposphere (warming in stratosphere) evolves for at least 2 to 3 years after the eruption. Furthermore, the volcanic aerosols serve as surfaces for heterogeneous chemical

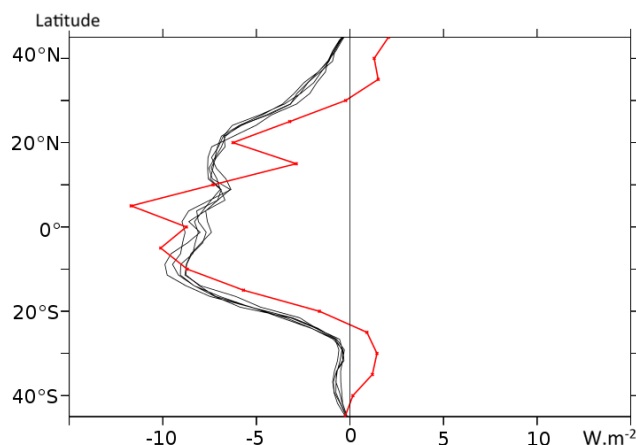


Fig. 1. Comparison of August 1991 absorbed shortwave radiative fluxes (SW, in W m^{-2}) at the top of the atmosphere (TOA) anomalies from Earth Radiation Budget Satellite (ERBS) observations (red) and 5 members simulation ensemble with the IPSLCM4v2 model (black). The simulated anomalies are computed as the differences between the Mt Pinatubo simulations and the control run. ERBS TOA SW radiative fluxes anomalies are expressed relatively to a 1985 to 1989 base climatology.

reactions that destroy stratospheric ozone, which controls solar energy absorption in the stratosphere. Its variations thus alter both the vertical temperature gradient between the troposphere and the stratosphere and the latitudinal temperature gradient in the stratosphere. We implemented in the IPSL model a new radiative module that mimics the direct radiative effect of sulphate aerosols. The input time series is based on the monthly mean optical thickness latitudinal reconstruction by Ammann et al. (2003) and Gao et al. (2008) from A.D. 850 to present. Vertically, the atmosphere in our model is divided into 19 hybrid sigma pressure levels with 4 layers above the tropopause. Due to the rather coarse vertical resolution, the optical properties of stratospheric sulfate aerosols in the visible band are evenly spread over the first two layers of the stratosphere. The optical properties were computed assuming a fixed sulfate aerosol droplet size distribution with a standard deviation of $1.8 \mu\text{m}$ and an effective radius of $0.5 \mu\text{m}$ corresponding to the average size of the Mt Pinatubo aerosols. As in Gao et al. (2008), all volcanic aerosols originate in the tropical band between 20°S and 20°N , where they last for few months, then spread poleward before decaying 3 years after the eruption started. As a validation, Fig. (1) shows the responses of reflected solar flux at the top of the atmosphere in August 1991, displayed as zonal averages between 40°S and 40°N in order to be comparable to Earth Radiation Budget Satellite (Minnis et al., 1993) in a series of sensitivity experiments. The model displays an overall agreement with the observations: shortwave anomalies associated with the volcanic eruption reaching 10 W m^{-2} between 10°S and 10°N in both model and observations.

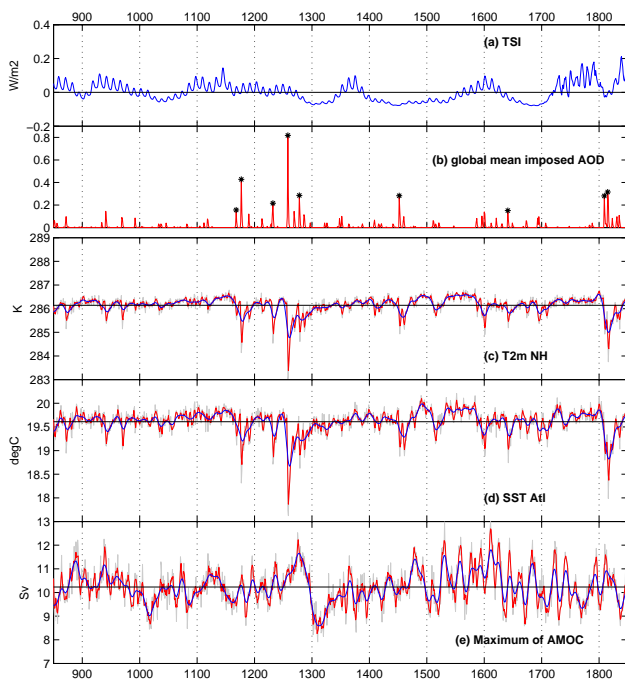


Fig. 2. Time series from 850 to 1850 of (a) Anomalous short wave input at the top of the atmosphere, taken as an estimation of variations of the TSI, (b) Imposed optical depth of volcanic aerosols. (c) Northern Hemisphere air temperature at 2 m (d) SST averaged between 30°S and 70°N in the Atlantic (e). Maximum of the meridional overturning circulation between 10°N and 60°N and below 500 m depth in the Atlantic. For c, d, and e, raw annual mean data are shown in grey and low pass filtered data using a running mean of 3 years in red. Low pass filtered data using a spline function with a cutoff at 20 years are shown in blue.

Figure (2) (second panel) illustrates the time series of implemented stratospheric volcanic aerosols optical depth. Note that a change in the global mean optical depth of 0.1 corresponds to a global anomalous radiative forcing of roughly -3 W m^{-2} . However, as discussed in Timmreck et al. (2009), the volcanic module tends to overestimate the radiative effect of the mega eruptions because of the use, for paleo-eruptions, of aerosol effective radius and optical depth derived from observations over the instrumental period, specifically for the Mount Pinatubo (1991) and El Chichón (1982) volcanic eruptions.

The greenhouse gas concentrations are those inferred from ice cores and direct measurements as reported in Servonnat et al. (2010). This simulation does not include the forcing by anthropic aerosols, so that global warming detected over the last decades of the simulation is overestimated (not shown). Hence, this study focuses on the natural external forcings and the period of investigation is limited to years 850 to 1849 A.D.

3 Temperature response to solar and volcanic forcings

Figure (2) also shows the air temperature at 2 m averaged over the Northern Hemisphere (third panel) and the SST averaged over the Atlantic Ocean (fourth panel). These time series highlight the fact that centennial variability is relatively weak in this simulation, and that some centennial features such as temperature shifts between the medieval climate anomaly (MCA) and the Little Ice Age (LIA) are not simulated in the model, unlike several reconstructions. Whether this is due to a model deficiency or the weak TSI variations is difficult to assess. We admit nevertheless that under TSI reconstructions with larger variations (Crowley 2000), the same model led to much larger SST low frequency variations, in relative agreement with paleoreconstructions, except for the onset of the MCA (Servonnat et al. 2010). The most striking signal in these time series are in fact important variations following volcanic eruptions, in particular an abrupt cooling of up to 3 °C in the atmosphere and 1 °C in the ocean. Such signature has also recently been found in temperature reconstructions in the subpolar North Atlantic (Sicre et al., 2011). On the other hand, variations of the solar insolation do not seem to have a strong imprint. The lagged correlation r of the anomalous TSI time series with the averaged surface air temperature in the Northern Hemisphere and with the Atlantic SST have a broad but weak maximum when the TSI leads by 4 years, reaching $r = 0.12$ and 0.13 , respectively (significant at the 5 % level) (Fig. 3). The corresponding correlation with the volcanic forcing is much larger, peaking when temperature lags by one year, with $r = -0.63$ and $r = -0.52$, respectively. For both air and sea temperature, the correlation with the volcanic signal remains significant for more than 15 years. Note that the significant correlation at lag -1 in Fig. (3) is due to the use of annual averages, as eruptions might in fact have started during the calendar year preceding the maximum of emission. The stronger influence of volcanic forcing is probably due to our use of a TSI reconstruction with weak variations and to an overestimation of the volcanic radiative effect (Sect. 2.2). In this sense, this simulation could be considered as a sensitivity study to volcanic eruptions over the last millennium.

The frequency dependence of the solar correlation is illustrated by the cross-wavelet coherence spectra in Fig. (4). The wavelet analysis was made with the Morlet wavelet, and the transform performed in Fourier space, using zero padding to reduce wraparound effects (Torrence and Compo 1998). The parameters were chosen to give a total of 57 periods ranging from 0.5 to 256 years, and the square coherency were calculated using smoothing in the time and space domain (Grinsted et al. 2004), with the 5 % significance level determined from a Monte-Carlo simulation of 1000 sets of surrogate time series. The two temperature time series show episodic coherency with the solar forcing at 11 year period (Fig. (4), top panels), in particular around 1200 and 1600. Meehl et al. (2008, 2009) indeed showed that a peak in

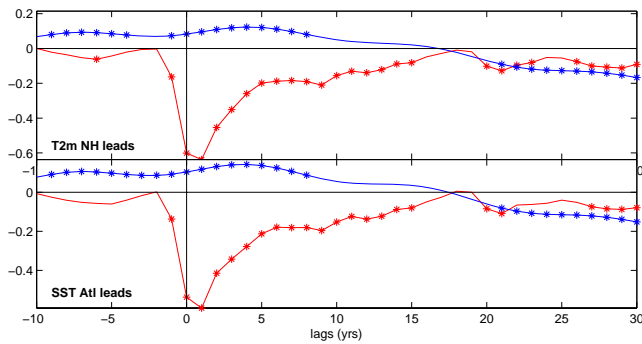


Fig. 3. Cross correlation between the temperature time series in Fig. 2 and the time series of the solar forcing (blue) and the volcanic forcing (red) from 850 to 1850 A.D. Lags with a star are significant at the 5 % level, tested against a bootstrap procedure with 500 permutation of the forcing time series using blocks of 3 years.

the solar activity induces surface cooling in the tropical Pacific. Kuroda et al. (2008) showed that over the historical period, years of anomalously high solar irradiance were associated with a large warming of the lower stratosphere through radiative heating. Such a temperature anomaly in the stratosphere creates anomalous temperature of opposite sign at lower heights. However, these processes require a much higher resolution in the stratosphere to be properly represented. In fact, episodic coherency between SST and TSI variations at 11 years timescale is also seen in the control simulation, suggesting that the significance test is too liberal. Signal in Fig. (4) is thus most probably internal to the data sets and does not indicate physical response of the ocean to the 11-year cycle. Furthermore, the 11-year cycle Fig. (2) (top) is primarily an extrapolation back in time of the 11-cycle observed in sunspots after year 1600. It is thus largely artificial. The temperature time series also show strong coherency with the TSI variations at multidecadal timescale from 1700, associated to the TSI increase, and at centennial time scales over the whole simulation (Fig. 4, second and third panels).

It is somewhat more difficult to distinguish the response of the Atlantic meridional overturning circulation (AMOC) from its natural variability. As shown in Fig. (2) (bottom panels), the AMOC intensifies during the second half of the thirteenth century, when volcanic activity was intense, peaks around year 1280 and then rapidly decreases, reaching a minimum around year 1320, about 60 years after the major eruption of 1260. There is a hint of a weak response to the eruptive events in the early 1800s. As shown in Fig. (4) (bottom), there is a hint of a weak coherence between the time series of AMOC maximum with the TSI variations at 11-year periods, but this is so sparse that such interpretation is debatable. There is a more significant coherence at about 100-year period, with TSI leading by 15 years (not shown). Correlations with the volcanic forcing are barely significant.

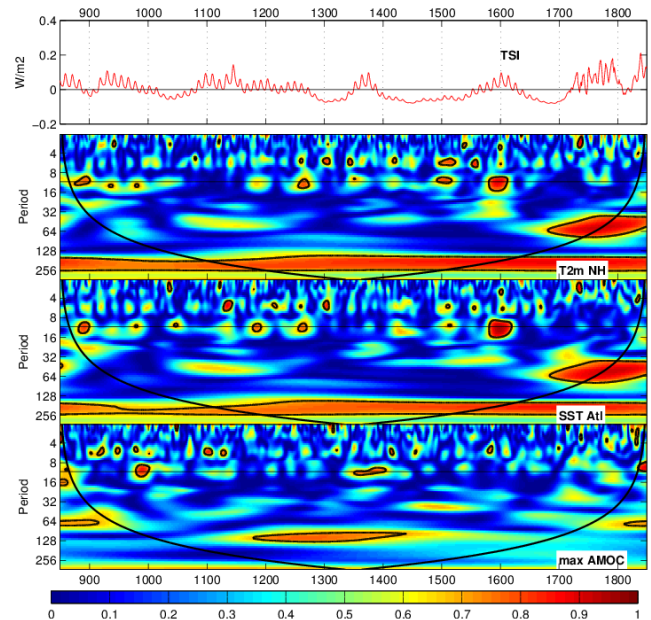


Fig. 4. Time series of the solar forcing (top) and cross-wavelet coherence spectrum of the temperature time series in Fig. 2 (bottom three panels). The thick contours enclose regions of greater than 95 % confidence and the thin lines indicate the limit of the cone of influence. The horizontal line indicates the 11 year period.

As will be shown below, this does not imply that there is no AMOC response to natural forcings, in particular volcanic eruptions. Time series of AMOC maximum represents one mode of AMOC variability, namely a basin scale acceleration, as discussed for example in Msadek and Frankignoul (2009). More local AMOC adjustments require more specific analysis. In the following, we concentrate on the response to volcanic forcing, which has a much stronger impact on the atmospheric and the oceanic temperature than the solar forcing in the model.

4 Anomalous temperature patterns in response to volcanic eruptions

To describe the oceanic response to a volcanic eruption, we construct a composite evolution based on the oceanic anomalies that follow the major eruptions. For each selected eruption, anomalies are computed as the difference between the time evolution of the field after the eruption and a reference defined as the average of the field during the two years preceding the eruption. A longer reference period would have the advantage to filter out inter annual climatic variability, but on the other hand, it would make the composites more sensitive to lower frequency variability. The choice of a shorter reference period was motivated by the focus of this study on the response of Atlantic Ocean circulation which is dominated by relatively long timescale variability. Note,

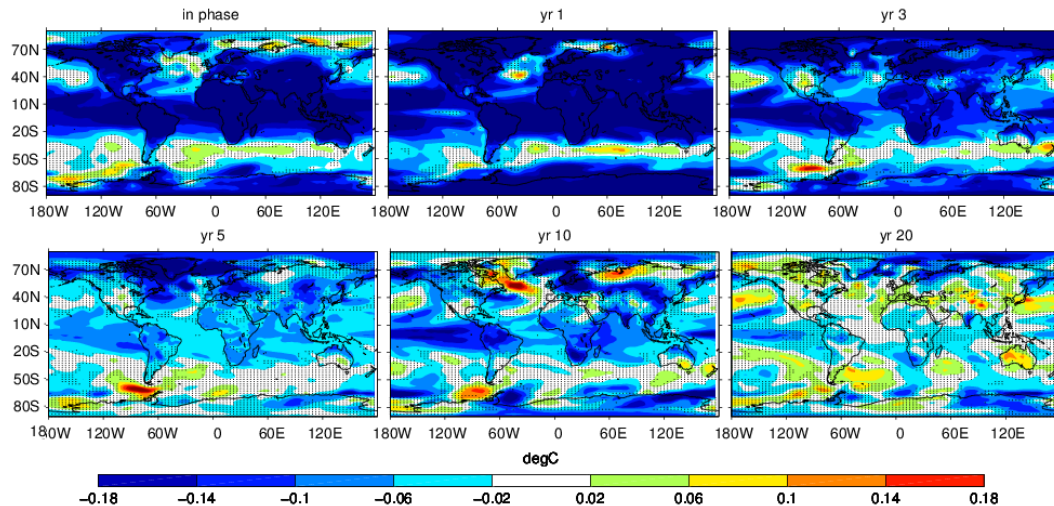


Fig. 5. Composites of annual mean anomalous surface temperature for different time lags (in years) with respect to the volcanic eruptions corresponding to optical depths higher than 0.15. Surface temperature corresponds to SST over the ocean and air temperature otherwise. Dotted areas are not significant at the 5 % level

however, that major results are unchanged for a reference period lasting up to five years prior to the eruption. Composites are then defined as the average of these anomalies scaled by the inverse of the magnitude of each eruption, so that possible non linear effects linked to the eruption magnitude are minimized. Note however that our conclusions are unchanged without this normalization. In order to maximize the signal to noise ratio, we focused on relatively large eruptions, and thus selected eruptions corresponding to an increase of stratospheric aerosol optical depth (AOD) by more than 0.15 (eruptions marked with a star in Fig. 2), which is equivalent to a global radiative forcing of at least -2.8 W m^{-2} . This corresponds to the 9 strongest eruptions between A.D. 850 and 1849. As seen in Fig. (2) and discussed in Sect. 2.2, several of the selected events follow each other by less than 10 years (1169–1178, 1810–1816). To minimize the interference between successive events, eruptions which precede another one by less than the considered time lag in the composite were omitted. As a consequence, the number of events in the composites may decrease with lag. The resulting composites are rescaled by 0.15 so that the amplitude of the results that are displayed are for an eruption with a stratospheric global mean optical depth equal to 0.15. Significativity is tested with a block bootstrap procedure with 500 permutations of the volcanic time series in blocks of 3 years (the maximum residence time of stratospheric aerosols). Composites are recomputed using each of these, resulting forcing time series in order so as to define the noise level.

Figure (5) shows composites of anomalous global annual mean surface temperature up to 20 years after a volcanic eruption of AOD of 0.15. The first panel (year 0) shows that the maximum cooling occurs in the tropics and on the lands during the year of the eruption. There is also a meridional dipole in the Southern Atlantic and the Indian oceans, which can be shown to be due to a shift of the westerlies, persisting for a year. In winter only, the anomalous winter warming over Eurasia consistent with the observations (e.g. Robock and Mao 1992) is significant at the 10 % level (not shown) and closely related to tropospheric and stratospheric circulation changes. As the lag increases, the tropical oceanic signal extends in latitude, reflecting the spreading of the atmospheric cooling (e.g. Robock 2000), while progressively decaying in the tropics. In the subpolar North Atlantic, the cooling peaks at year 3 and decays thereafter. Note the relatively rapid decay of the cooling in the eastern equatorial Pacific at year 1, also present at year 2 (not shown) which could be due to an El Niño-like response. One to two years after the eruption, there is an anomalous warming in the North Atlantic midlatitudes, the origin of which is discussed below. An anomalous warming near the Drake Passage becomes significant at year 3 and reaches its maximum at year 5. Ten years after the eruption, the whole tropical band is still significantly anomalously cold, as well as some land areas such as in Eurasia. In the North Atlantic, the most striking feature is an anomalous warming in the Labrador Sea, which decays thereafter.

Figure (6) shows similar composites for the zonally averaged global oceanic temperature response as a function of depth up to 20 years after a volcanic eruption. Consistent with Fig. (5), a temperature decrease of up to 0.25 K appears

in the upper tropical ocean during the eruption year, together with a warming below 100 m depth in the deep tropics. The latter results from a thickening of the tropical thermocline and a decrease of equatorial ventilation following a weakening of the trade winds, as discussed below. The surface cooling already reaches 60° N, but its poleward extension is stronger one year after the eruption, consistent with Fig. (5). By year 1, the signal has penetrated in the ocean interior around 30° N and 30° S, where oceanic ventilation mostly takes place. In the subtropics, the downwelling is shifted slightly poleward of the climatological ventilation region, indicated by the mean isotherms in Fig. (6) (white contours). As in Laurian et al. (2009), the shift can be explained by the poleward displacement of the surface isopycnals resulting from the surface cooling. Deep penetration down to 900 m of the cooling is also seen around 60° N at year 1, reflecting enhanced deep convection. Deep convection also mixes the cooling signal down in the Southern Ocean, reaching its largest depth 2 to 3 years after the eruption (not shown). In the following years, the tropical surface cooling decays, while persisting at depth and deepening further (Fig. (6), year 5). As the surface cooling reaches greater depths, the subsurface warming deepens and shifts poleward.

After 10 years, the cooling signal has reached more than 500 m at 40° latitude north and south, which is roughly the maximum depth of the subtropical cells, and 700 m in the Southern Ocean. In the North Atlantic, on the other hand, a warm subsurface anomaly has appeared, reflecting a decrease of deep convection as will be discussed below. At this stage, the response is thus asymmetric in the high latitudes as also found by Stenchikov et al. (2009). Twenty years after an eruption, cooling is still significant in the tropics and at high latitudes, where it reaches 700 to 900 m, while the northern subtropics have warmed, reflecting the dynamical adjustment of the gyres discussed below.

In the following, we focus on the response of the Atlantic Ocean, as a case study and in order to investigate the behavior of the AMOC. From Fig. (2), it seems clear that the behavior of the AMOC after the severe and decadal paced eruptions of the twelfth and thirteenth century is peculiar. Figure (7) illustrates the different response of the ocean to the selected eruptions occurring after 1400, from the ones occurring between 1100 and 1300. In high response to volcanic eruptions occurring after 1400 (bottom panels), the initial (in phase) cooling is more clearly limited to the tropics and subtropics, while the mid and high latitudes are characterized by an anomalous warming, due to anomalous turbulent heat fluxes as discussed below. The anomalous cooling rapidly reaches the higher latitudes (yr 1 to 4), except for a small patch of anomalous warming at 45° N which reflects a northward shift of the North Atlantic Current. After about a decade, the anomalous cooling has disappeared or lost significance in the Atlantic basin, while a strong and persistent warming has appeared in the subpolar gyre, with maximum amplitude south of Greenland, and extends in the

Table 1. Month of maximum global mean AOD for the selected eruptions. The input time series is based on the monthly mean optical thickness latitudinal reconstruction by Ammann et al. (2003) and Gao et al. (2008).

Period 1100–1300		Period 1400–1850	
eruption year	month of maximum AOD	eruption year	month of maximum AOD
1168	February	1452	May
1177	February	1641	May
1231	November	1809	May
1258	April	1815	September
1278	May to October		

eastern subtropics in a coma shape which resembles the path of the subtropical gyre. This horseshoe-like structure thus is strongly similar to the signature of an AMOC acceleration in the coupled model (e.g. Msadek and Frankignoul 2009).

On the other hand, the anomalous cooling occurring in phase with the intense and decadal paced eruptions between 1100 and 1400 is significant not only in the tropics, but also at subpolar latitudes, in particular in the Irminger Sea and the Nordic Seas, where deep convection in the model takes place. There is also a weak, marginally significant, warming at midlatitude, again probably reflecting a shift in the North Atlantic current, but it is short lived and the entire basin becomes anomalously cold in the years following the eruption. At decadal timescales, the anomalous subpolar warming seen after 1400 can be recognized but it is much weaker and not significant at the 5% level. The fact that the response differs already in phase with the eruption suggests an immediate difference and tends to eliminate the cumulative effect of the decadal-paced eruptions of the twelfth and thirteenth century, as opposed to more isolated eruptions occurring after year 1400. A larger signal to noise ratio in response to stronger eruptions might be an alternative explanation, as discussed e.g. in Shindell et al. (2003) and Schneider et al. (2009). However, the anomalous atmospheric response shown in Fig. (7) (top) is unchanged if the mega eruption of 1258–1259 is omitted for the computation of the composite (not shown). Table 1 suggests rather that the eruptions of the middle age period tend to peak during the cold season, while the ones that occurred during the rest of the last millennium mostly peak during the warm season. Nevertheless, given the relatively strong uncertainty in this seasonality in the reconstruction (Gao et al. 2008), this is quite hypothetical. Investigating the effect of this seasonality requires specific sensitivity experiments and is beyond the point of this study. Finally, Fig. (2) (bottom) suggests that the AMOC variability has a different character pre and post 1300, with more high-frequency variability in the later period, especially after 1500. Whether this could explain some part of the difference will be discussed in the conclusion. Note however that

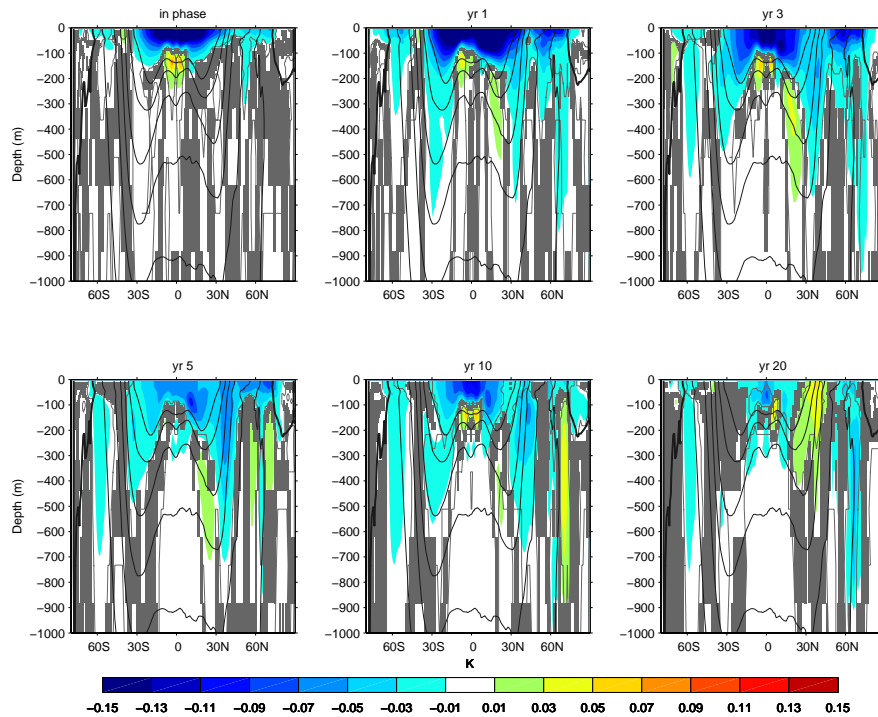


Fig. 6. Composites of anomalous zonally averaged oceanic temperature response at different time lags (in years). Shaded areas are not significant at the 20 % level. Grey contours indicate anomalies significant at the 5 % level. Dark contours show the zonal mean global temperature (contour interval is 3 °C).

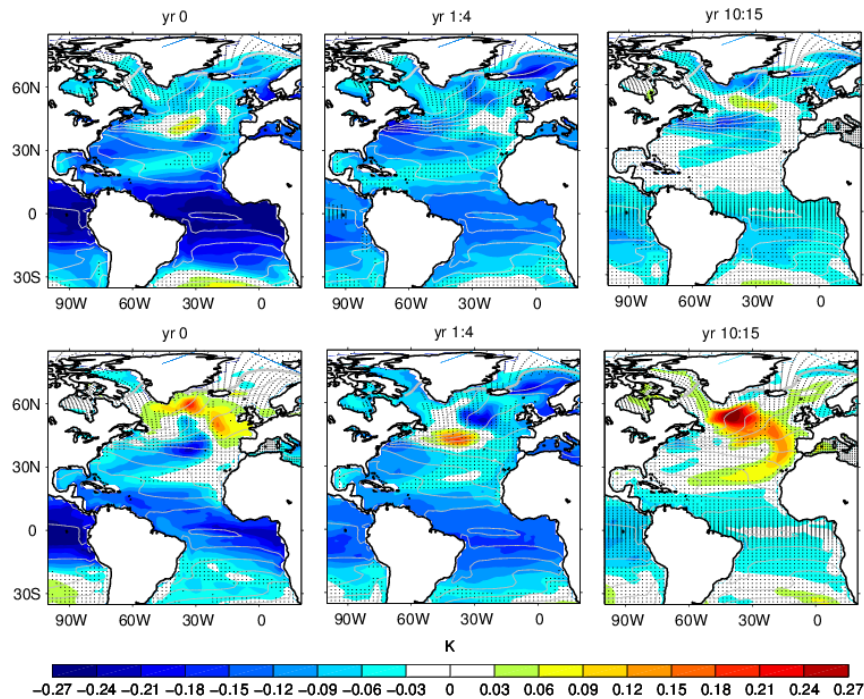


Fig. 7. Composites of anomalous sea surface temperature following volcanic eruptions in different periods. Top: between 1100 A.D. and 1300 A.D., bottom: after 1400 A.D. Dotted areas are not significant at the 5 % level. Grey contours show the annual mean SST. Contour interval is 3 K, the thick line is for the zero contour.

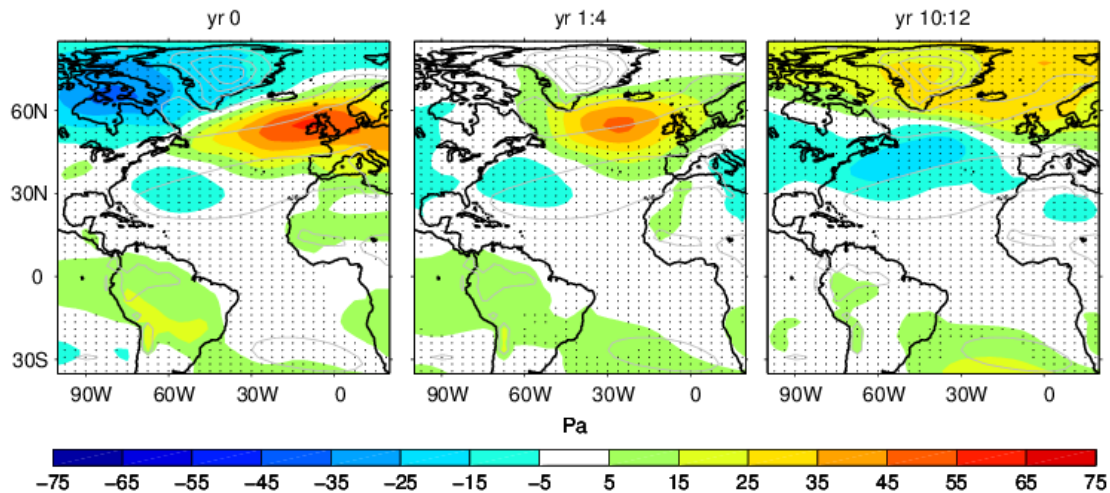


Fig. 8. Composites of annual mean anomalous sea level pressure in phase with the volcanic eruption (left) and following the volcanic eruption (other panels) for the period after 1400 A.D. Grey contours show the SLP annual mean in the model (contour interval is 10^2 Pa)

Zanchettin et al. (2011) also noted modulation of volcanic-forced perturbations by the background climate. In the following, we will first investigate the response to eruptions occurring after 1400.

5 Interannual to decadal response of the Atlantic Ocean to eruptions post 1400 A.D.

In response to the rapid surface cooling, there is a strong anomalous low over the Canadian Archipelago and an anomalous high over the northeastern Atlantic. In addition, the sea level pressure (SLP) becomes anomalously high over South America and most of Africa, where the cooling is strongest, and an anomalous low in the western subtropics (Fig. 8). Consequently, the Northern Hemisphere trades and westerlies are reduced during the year of the eruption, and shifted southward. Over the tropical lands, the SLP signal weakens at year 1, but it remains significant for almost 2 decades over the Amazonian Basin. At mid to high latitudes, the anomalous low quickly disappears but the anomalous anticyclone shifts slightly westward and persists until year 4, resembling a negative phase of the East Atlantic Pattern (EAP). Later, the signal loses significance (not shown), until year 10, where a response resembling a negative phase of the NAO is detected.

At year 0, the wind changes induce a negative wind stress curl anomaly across the basin between 50 and 60° N and a positive one north and south of it (Fig. 9, left). The depth-integrated oceanic circulation, as described by the barotropic streamfunction, adjusts rapidly to the wind stress curl. At year 0, it is anomalously negative in much of the subtropical Atlantic, reflecting a weakening of the subtropical gyres

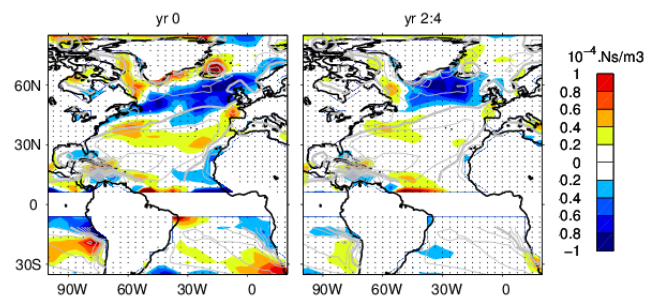


Fig. 9. Composites of anomalous wind stress curl, shown over oceans only, in phase with the volcanic eruption (left) and following the volcanic eruption by two to four years (right) for the period after 1400 A.D. Grey contours show the annual mean values (contour interval is 10^{-4} $Ns\ m^{-3}$), the thick grey line shows the zero contour.

(Fig. 10, left). A weak positive anomaly is also significant in the subpolar region, where the wind stress curl is negative. At following lags, the negative wind stress curl anomaly persists at subpolar latitudes and shifts to the southern Irminger Sea, consistent with the SLP response (Fig. 9, right). Two to four years after the eruption, both gyres of the North Atlantic are thus clearly reduced. At longer lags, the response decays in the subtropics while the subpolar gyre stays anomalously weak for more than a decade after the eruption (Fig. 10, middle). Note also the persistent signal in the Labrador Sea where the cyclonic circulation is reinforced.

The atmospheric response to the eruption also induces vertical circulation in the ocean, resulting from the anomalous Ekman suction at 30° N/S and pumping around 50° N. This appears clearly at year 0 on the meridional streamfunction

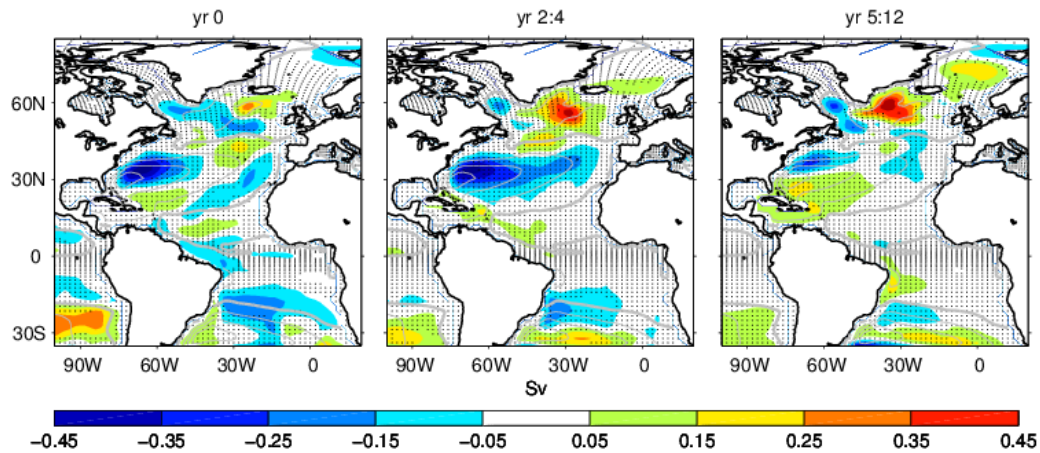


Fig. 10. Composites of anomalous Atlantic barotropic streamfunction in phase with the volcanic eruption (left) and following the volcanic eruption (other panels) for the period after 1400 A.D. Positive (negative) values correspond to an anticyclonic (cyclonic) circulation. Grey lines show the annual mean stream function in the model, with a contour interval of 10 Sv

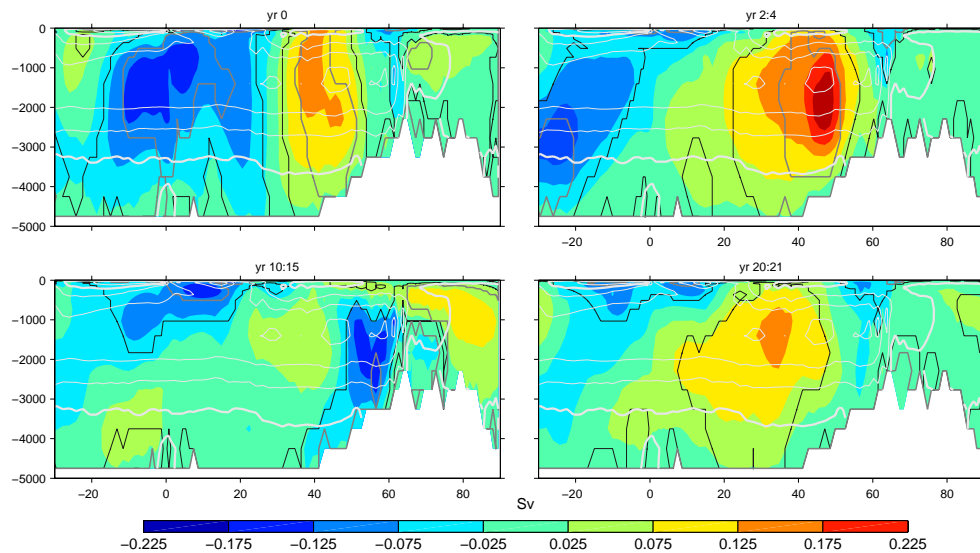


Fig. 11. Composites of anomalous Atlantic meridional streamfunction in phase with the volcanic eruption (left) and following the volcanic eruption (other panels) for the period after 1400 A.D. Positive (negative) values correspond to a clockwise (counter-clockwise) circulation. Black and grey contours mark significant areas at the 95 % and 80 % level, respectively, according to the Monte Carlo permutation test. Light grey contours show the annual mean Atlantic meridional circulation in the control simulation (contour interval is 3 Sv, thick contour corresponding to the zero contour.)

composite (Fig. 11, left). The signal is equivalent barotropic, with an upwelling around 30° N and a downwelling at 50° N and around the equator. During the following years, the strong negative wind stress curl in the subpolar North Atlantic maintains a positive meridional cell between 20 and 50° N, which can be viewed as an intensification of the AMOC in the North Atlantic, consistent with previous studies (e.g. Stenchikov et al. 2009, Ottera et al. 2010, Ortega et al., 2011). Note that this positive anomaly is probably

also favored by the intensified deep convection that occurs during the year of the eruption (Fig. 12, top), and is associated with strong surface cooling. An intensification of deep convection typically leads by several years an acceleration of the AMOC in the North Atlantic Basin (e.g. Mignot and Frankignoul 2005). However, it is short-lived here, losing significance by year 1, so that the AMOC intensification does not persist more than a few years (Fig. 11, bottom left). On the other hand, there is a weak reduction of the AMOC north

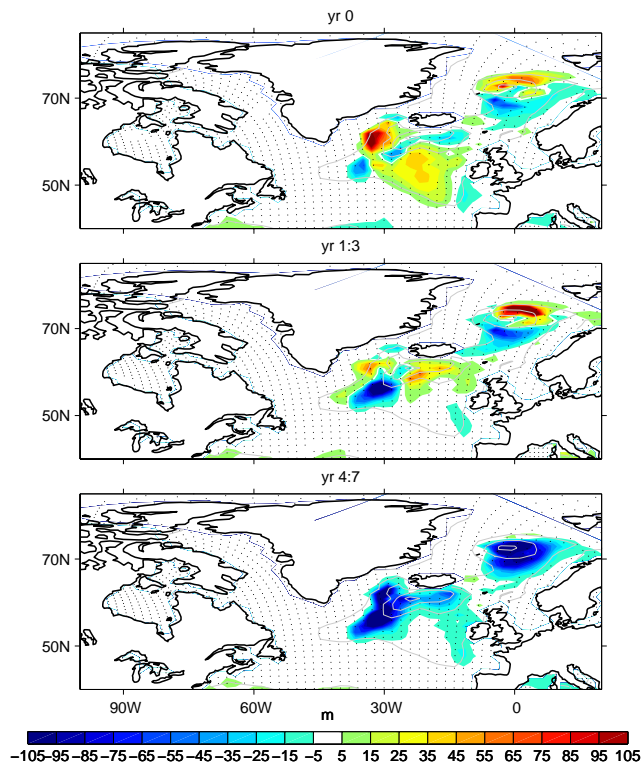


Fig. 12. composites of anomalous March mixed layer depth during the year of the eruption (left), averaged over the following 3 years (middle), and averaged 4 to 7 years later (right) for the period after 1400 A.D. Grey lines show the annual mean mixed layer depth field in the model, with a contour interval of 500 m

of about 60° N up to four years after an eruption, which later intensifies and extends to subpolar latitudes as a result of a reduction in deep water formation, as discussed below.

Five years after the volcanic eruption, the SLP anomaly decreases (not shown). Nevertheless, as indicated above, a significant SLP anomaly appears again near year 10–12, under the form of the dipole in the mid to high latitudes bearing similarity with a negative phase of the NAO. This could reflect the SLP response to the AMOC intensification seen at year 2–4 (Fig. 8 upper right), since Gastineau and Frankignoul (2011) found a weak but significant response of the atmosphere (negative NAO phase) to enhanced AMOC in several climate models including the control simulation with IPSLCM4. In the latter, the SLP response was of similar magnitude and most clearly seen four years after an AMOC intensification. Here, the AMOC intensification indeed remains significant until lag 8 (not shown) Whether there is a link with the weak AMOC intensification seen about 20 years after the eruption cannot be asserted here but could be established in dedicated experiments. As mentioned above, the strong surface cooling rapidly deepens the mixed layer south of Iceland (Fig. 12, top panel) and in the subtropics (not

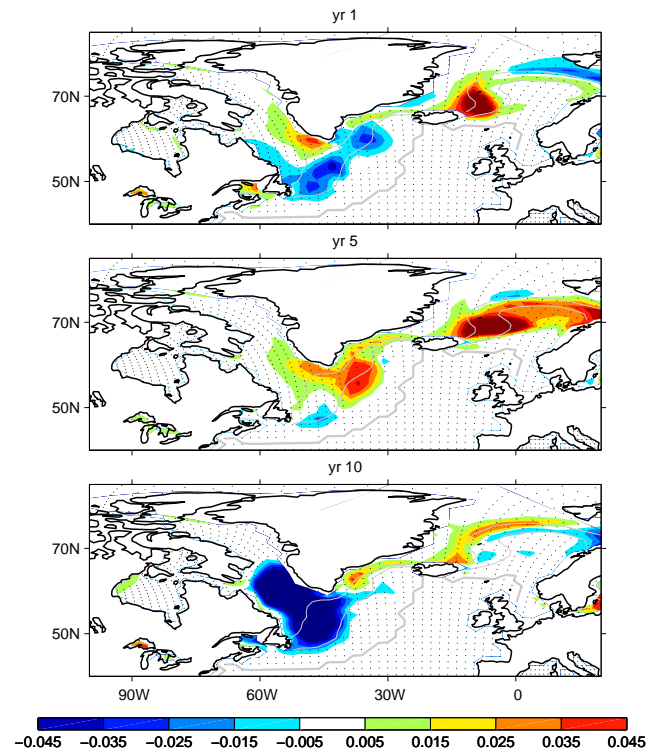


Fig. 13. composite of anomalous March sea ice cover during the year following the eruption (left), 5 years later (middle), and 10 years later (right) for the period after 1400 A.D. Grey lines show contours of the average sea ice cover in March of 0, 0.5 and 1.

shown). The intensification of deep convection favors the penetration of the cooling signal at depth seen in Fig. (6) at high northern latitudes and a weakly significant retreat of sea ice cover (Fig. 13, left panel). However, this response loses significance in the following years (Fig. 12, middle panel), and instead, deep convection is reduced both in the Nordic Seas and South of Iceland 4 years after an eruption (Fig. 12, bottom panel). This persists for about a decade after the eruption. In the Nordic Seas, the reduction of deep convection is due to a persistent sea ice capping of the area during winter, resulting from the strong surface cooling (Fig. 13). This anomaly appears about 1 year after the eruption, peaks after four years and, again, persists for roughly a decade. Such anomalous sea ice extension is consistent with the sea ice reconstruction off Iceland from Masse et al. (2008), showing abrupt events that coincide with the volcanic eruptions after 1300 A.D.

South of Iceland, the winter mixed layer shallowing in Fig. (12) (bottom) is due to a strong negative salinity anomaly (Fig. (14) top). The latter is largely due to anomalous Ekman transport (Fig. (14), bottom), while anomalous atmospheric freshwater fluxes play a lesser role (Fig. (14), middle), consistent with Mignot and Frankignoul (2003, 2004). Note that the anomalous surface freshwater flux

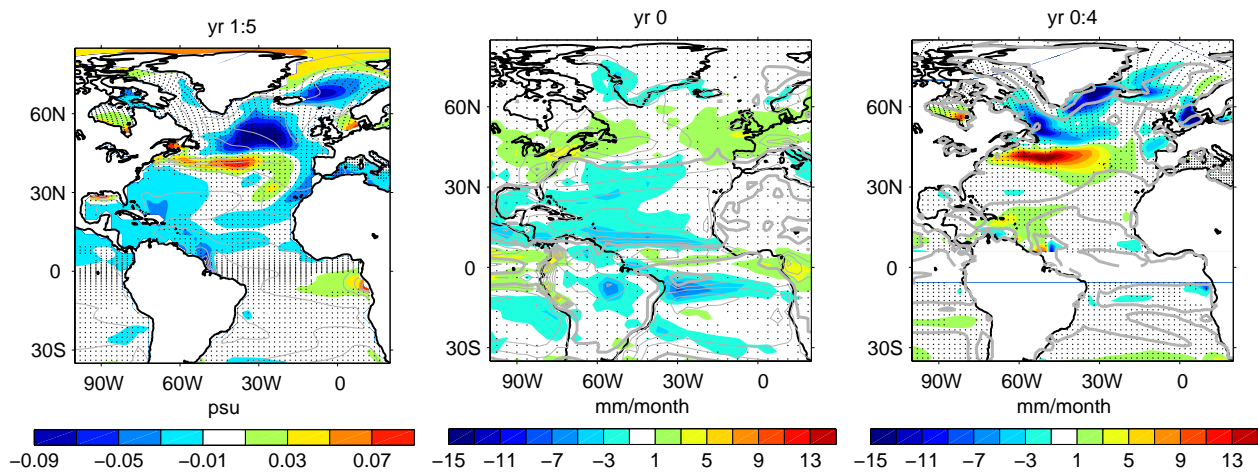


Fig. 14. Top: Composites of anomalous SSS averaged 1 to 5 years after the eruption. Grey lines show the annual mean SSS field in the model, with a contour interval of 2 psu. Middle: Composite of anomalous E-P during the year of the eruption. Bottom: composite of advection of mean salinity by anomalous Ekman currents (with a negative sign in order to be consistent with the E-P forcing term) averaged over the 4 years following the eruption. Values equatorward of 10° latitude are masked because undefined. All composite are computed for eruptions occurring later than 1400 A.D. For the two right panels, grey lines show the annual mean field in the model with a contour interval of 40mm/month. The zero contour is thicker. For all panels, dotted areas are not significant at the 5 % level.

caused by the volcanic eruptions are maximum during the year of the eruptions, and in the tropics (Fig. 14), consistent with Trenberth and Dai (2007). The reduction of the northern trade winds (Fig. 8) is indeed associated to a northward shift in the inter-tropical convergence zone. As a result, precipitation is enhanced near 10° N and strongly reduced along the equator, including over the continents. In the northern deep tropics, evaporation is reduced, again because of reduced winds and SST. These anomalous surface freshwater fluxes induce the negative salinity anomaly in the northern subtropics in the years following the eruption.

6 Interannual to decadal response of the Atlantic Ocean to eruptions between 1100 and 1300

Figure (15) shows the response of the AMOC to the volcanic eruptions selected during the period of intense volcanic activity between 1100 and 1300. As during the later period, the in-phase response is essentially characterized by an anomalous upwelling around 30° N. The associated negative and positive cells south and north of this latitude have nevertheless a much weaker extension in depth (for the tropical one) and in latitude (for the northern one) than for the later period. Indeed, the anomalous sea level pressure induced during the year of an eruption occurring during the earlier period, shown in polar view in Fig. (16), is similar in the tropics and subtropics (not shown) but it has the opposite sign over the Canadian Archipelago and there is no strong high in the eastern North Atlantic. As a result, the anomalous wind stress curl is much weaker in the subpolar region, inducing a much weaker

anomalous Ekman pumping and Ekman transport, and only little salt advection (not shown). The subpolar gyre is thus much less affected during the years following the eruption (not shown). Lacking the large subpolar freshening seen in the later period, the winter mixed layer remains anomalously deep in the subpolar region (Fig. (17) middle panel), even further south than deep convection locations, due to the surface cooling (Fig. 7), which might contribute to the broad and shallow AMOC intensification between 20° S and 45° N at years 2 to 4. It can be shown that the tropical part of this anomalous cell is associated with an equatorward shift of the subtropical gyre. On the other hand, deep convection is reduced in the Nordic Seas after a few years because of the sea ice capping discussed above. Note that in this period, the anomalous sea ice extension develops faster and it is stronger and more persistent (Fig. 18) than in the later period, consistent with the stronger cooling (Fig. 7). It is also interesting to note that the weak gyre response also contributes to maintain the oceanic surface cooling in the 1100–1300 A.D. period, since it does not induce the warm anomaly seen in the years following an eruption occurring after 1400 A.D. (Fig. 7). As a result, the negative AMOC anomaly seen over the ridges two to four years after an eruption is stronger and deeper than for the eruptions occurring after 1400 A.D. After a longer delay, when anomalous cooling and convection in the subpolar basin start to vanish, the shallowing of the winter mixed layer in the Nordic Seas seen at years 4–7 in Fig. (17) (bottom) persists and is likely responsible for the stronger negative AMOC weakening seen throughout the northern North Atlantic at least two decades after the eruptions (Fig. (15), bottom left). This behavior is consistent with

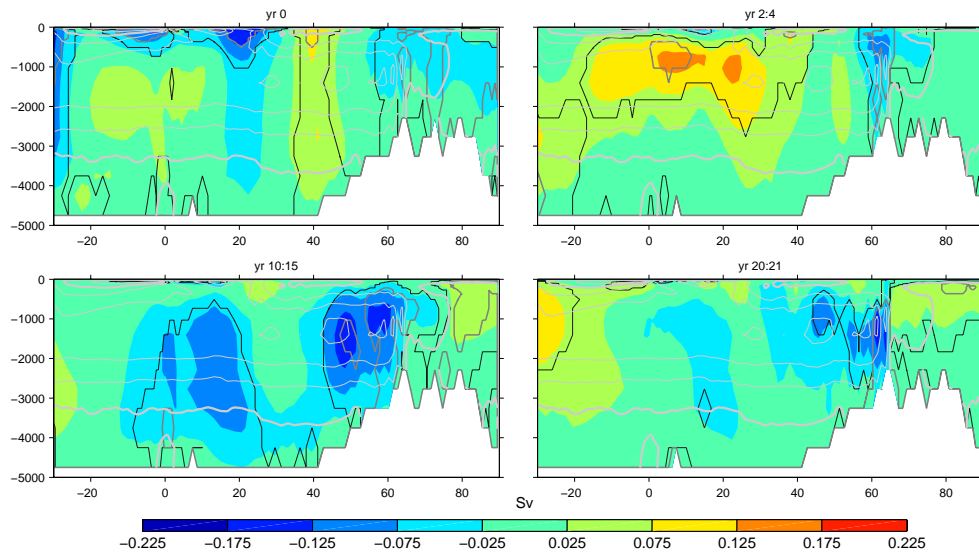


Fig. 15. As in Fig. 11 for the Atlantic meridional streamfunction during the period 1100–1300. Positive (negative) values correspond to a clockwise (counter-clockwise) circulation. Black and day grey contours mark significant areas at the 95 % and 80 % level, respectively, according to the Monte Carlo permutation test. Light grey contours show the annual mean Atlantic meridional circulation in the control simulation (contour interval is 3 Sv, thick contour corresponding to the zero contour.)

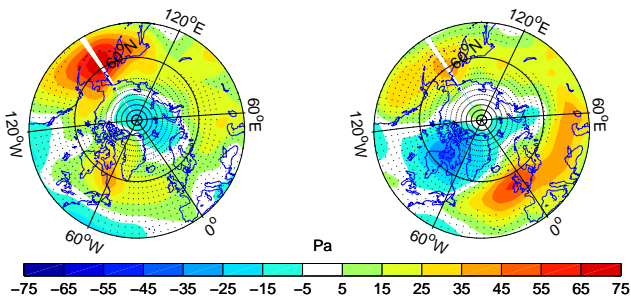


Fig. 16. composite of annual mean anomalous sea level pressure in phase with the volcanic eruptions of the period 1100–1300 A.D. (left) and with the volcanic eruptions post-1400 A.D. (right).

Zhong et al. (2010). That the AMOC weakening extends north of the ridges adds credit to the implied role of Nordic Seas convection and could explain why the AMOC behavior has become nearly opposite to that seen after 1400 A.D.

7 Conclusions and discussion

In this study, we have investigated the oceanic response to volcanic eruptions over the last thousand years, with a focus on the North Atlantic Ocean. We used a fully coupled AOGCM forced by a realistic chronology of volcanic eruptions, variations of the TSI and of the atmospheric greenhouse gases concentrations. Note that the TSI reconstruction chosen to force the model is relatively weak, and that some

centennial features suggested by observations, such as temperature shifts between the medieval climate anomaly and the Little Ice Age, are not simulated in the model. In this sense, this simulation can be considered as a sensitivity simulation to the volcanic eruptions over the last millennium. Nevertheless, as far as the response of the ocean to intermittent and sudden volcanic events does not depend too strongly on the average temperature, this caveat does not invalidate our study. The analysis highlighted the multiple timescales of the response, including a fast tropical temperature adjustment to the strong volcanic-induced radiative forcing, dynamical adjustment in response to the associated atmospheric circulation modifications persisting roughly 5 years, and a subsequent adjustment of the AMOC in response to anomalous convection at high latitudes. The analysis also highlighted differences in the response during two distinct periods of the last millennium.

The global surface temperature response is maximum one to two years after a volcanic eruption. The anomaly penetrates at depth via subtropical oceanic ventilation as well as deep convection at high latitudes. It thus persists globally in the ocean for more than 20 years. During the year of the eruption, anomalous tropical cooling induces an anomalous high over the continents and a reduction of the trades in the Atlantic Ocean. The atmospheric response at mid to high latitudes depends on the eruptions. In this study, in order to investigate apparent discrepancy found in the literature regarding the AMOC response, we only separated eruptions occurring after 1400 from the ones occurring between 1100 and 1300. In the later period, the anomalous atmospheric

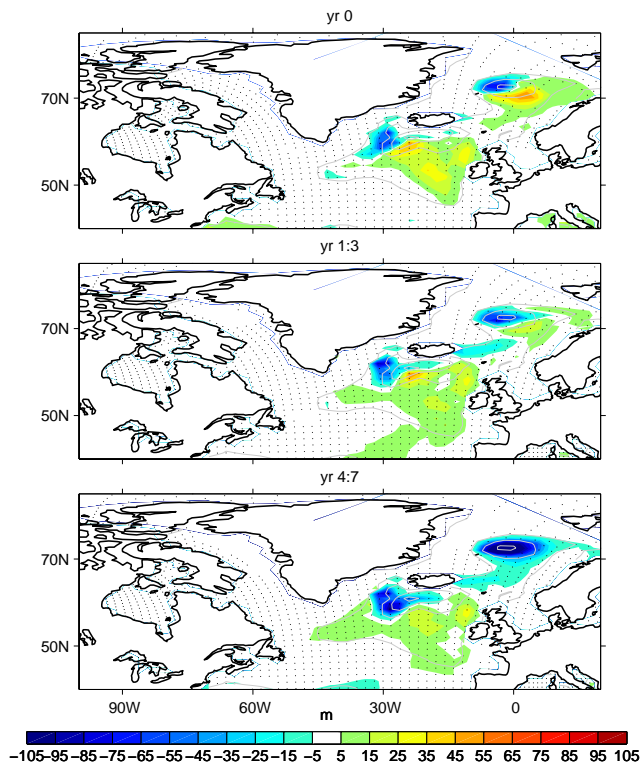


Fig. 17. Composites of anomalous March mixed layer depth in response to volcanic eruptions occurring during the period 1100–1300. The composite is shown for the year of the eruption (left), averaged over the following 3 years (middle), and averaged 4 to 7 years later (right). Grey lines show the annual mean mixed layer depth field in the model, with a contour interval of 500 m. Dotted areas are not significant at the 5% level.

structure in response to an eruption induces strong wind stress curl anomalies over the North Atlantic Ocean, which lead to an important dynamical adjustment in the Atlantic Ocean at interannual timescales, namely one to five years after an eruption. This adjustment of the oceanic circulation is equivalent barotropic, with an upwelling around 30° N and a downwelling at 50° N and around the equator. The anomalous vertical oceanic circulation can reach the full depth of the ocean. During the following years, the atmospheric structure evolves inducing an anomalous acceleration of the AMOC in the subpolar basin. However, this anomaly does not persist more than a few years, because of reduced deep convection in the high northern latitudes under the effect of anomalous sea ice extension and surface freshening that develop a few years after the eruption. A weak reduction of the AMOC is thus detected a decade after the eruption. In the case of the eruptions occurring between 1100 and 1300, the anomalous SLP structure during the year of the eruption differs over the subpolar region from the one obtained during the later period. It induces much weaker wind stress curl anomalies over the Atlantic basin and thus a much weaker

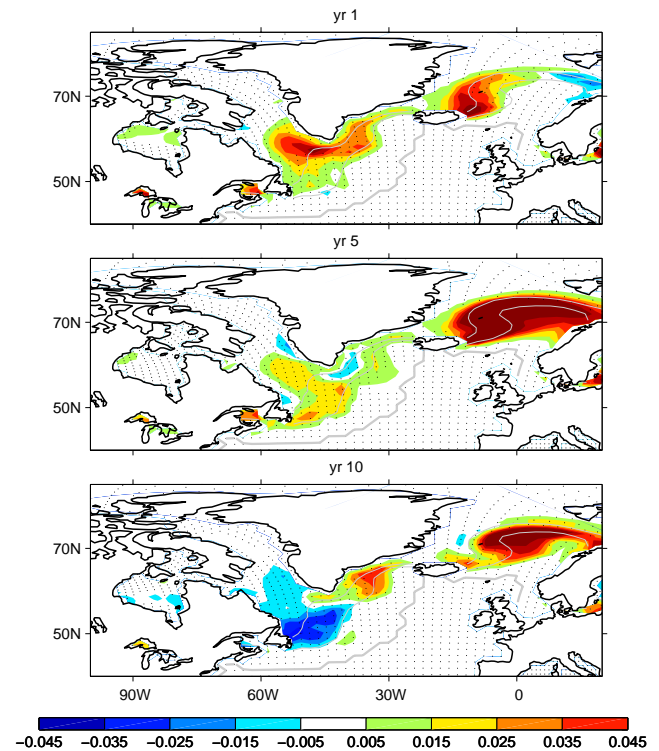


Fig. 18. Composites of anomalous March sea ice cover in response to volcanic eruptions occurring during the period 1100–1300. The composite is shown for the year following the eruption (left), 5 years later (middle), and 10 years later (right). Grey lines show contours of the average sea ice cover in March of 0, 0.5 and 1. Dotted areas are not significant at the 5% level.

dynamical adjustment of the AMOC in the years following an eruption. On the other hand, the initial reduction of deep water formation is more persistent, as a result of a stronger surface cooling and more persistent sea ice cover anomalies, leading to a stronger negative anomaly of AMOC at high latitudes 2 to 4 years after an eruption, and a stronger reduction of the AMOC in the subpolar North Atlantic 10 to 15 years after the eruption.

As noted in the introduction, the oceanic response to volcanic eruptions is still largely unknown and recent studies based on climate models suggest either an AMOC enhancement or a reduction following volcanic eruptions of the last millennium. The present findings could possibly reconcile these previous studies, suggesting a strong sensitivity of the response to different volcanic eruptions. In particular, the AMOC intensification seen 5 to 10 years after the volcanic eruptions occurring after 1400 A.D. bears strong similarity with results of Ottera et al. (2010) using a different coupled climate model to investigate this period. On the other hand, the AMOC weakening in the northern North Atlantic and the large sea ice extension following the intense eruptions occurring between 1100 and 1300 can be compared to the response found by Zhong et al. (2010). Investigating the whole last

millennium, Zanchettin et al. (2011) noted a general AMOC intensification but note also a modulation of this response with the background state. The present analysis suggests that these different responses involve in fact similar mechanisms, namely an initial dynamical adjustment to anomalous winds and a subsequent thermohaline response to anomalous deep convection. However, the atmospheric response to the volcanic eruptions differ in the two periods and thus plays a large role in modulating the oceanic response. At least three factors could explain why the atmospheric response seems to change in time: the seasonality of the eruption, its intensity, and the cumulative effect in the case of successive eruptions. An analysis of these various effects requires specific experiments that are left for future studies. However, the results presented here suggest that the seasonality is a plausible explanation. Indeed, the eruptions during 1100–1300 occurred mostly during the cold season while those after 1400 occurred mostly during the warm season. Although cumulative effects may also play a role, they cannot explain why the short term response already differs in the two periods. Nonlinearities in the response could also be important, even though our results were not changed when the mega eruption of 1258 was omitted from the 100–1300 composite. Finally, since different responses of SLP and AMOC to eruptions pre and post 1400 occur as soon as the year of the eruption, the change in interannual variability pointed out in Fig. (2) (bottom panel) is probably not the cause.

Other features of the oceanic response to the eruptions can be compared to previous studies. The important role of sea ice dynamics was also noted by Stenchikov et al. (2009), Zhong et al. (2010) and Zanchettin et al. (2011). The response of the barotropic stream function bears also some interesting similarities with Zanchettin et al. (2011), including an initial response dominated by a shift of the gyres (or an inter gyre gyre in their framework) and a later response dominated by an intensification of the subpolar gyre. Generally, both studies highlight an initial dynamical response to atmospheric circulation and a subsequent decadal adjustment of the ocean. Comparison among these results also calls for a coordinated comparison of simulations of the last millennium.

The oceanic response is also likely to be affected by model biases and experiment design. In particular, the lack of deep convection in the Labrador Sea in the IPSLCM4 model is probably a major drawback. A better representation of the stratosphere is also needed to improve the representation of the effect of volcanic aerosols. Indeed, stratospheric dynamics and chemistry may significantly alter the modeled climatic impact of volcanic eruptions. This should be tested in the new version of the IPSL model including 39 atmospheric levels and an improved radiative module, currently under development, as well as in the forthcoming CMIP5 database.

Acknowledgements. The simulations used in this study have been run in the framework of ANR- ESCARSEL (2007–2011). The research leading to these results has received funding from the European Community's 7th framework program (FP7/2007–2013) under grant agreement No. GA212643 (THOR: "Thermohaline Overturning – at Risk", 2008–2012). Stimulating discussions with M.A. Sicre are gratefully acknowledged.

Edited by: U. Mikolajewicz



The publication of this article is financed by CNRS-INSU.

References

- Ammann, C., Meehl, G., Washington, W., and Zender, C.: A monthly and latitudinally varying volcanic forcing dataset in simulations of 20th century climate, *Geophys. Res. Lett.*, 30, 1657, doi:10.1029/2003GL016875, 2003.
- Ammann, C., Joos, F., Schimel, D., Otto-Bliesner, B., and Tomas, R.: Solar influence on climate during the past millennium: Results from transient simulations with the NCAR climate system model, *Proc. Nat. Acad. Sci. USA*, 104, 3713–3718, doi:10.1073/pnas.0605064103, 2007.
- Church, J., White, N. J., and Arblaster, J. M.: Significant decadal-scale impact of volcanic eruption and sea level and ocean heat content, *Nature*, 438, 74–77, doi:10.1038/nature04237, 2005.
- Crowley, T.: Causes of climate change over the past 1000 years, *Science*, 289, 270–277, doi:10.1126/science.289.5477.270, 2000.
- Fichefet, T. and Maqueda, M. A. M.: Sensitivity of a global sea ice model to the treatment of ice thermodynamics and dynamics, *J. Geophys. Res.*, 102, 12609–12646, doi:10.1029/97JC00480, 1997.
- Foukal, P., North, G., and Wigley, T.: A stellar view on solar variations and climate, *Science*, 306, 68–69, doi:10.1126/science.1101694, 2004.
- Gao, C., Robock, A., and Ammann, C.: Volcanic forcing of climate over the last 1500 years: An improved ice-core based index for climate models, *J. Geophys. Res.*, 113, D2311, doi:10.1029/2008JD010239, 2008.
- Gastineau, G. and Frankignoul, C.: Cold-season atmospheric response to the natural variability of the Atlantic meridional overturning circulation, *Clim. Dyn.*, in press, 2011.
- Gleckler, P., Wigley, T. M. L., Santer, B. D., Gregory, J. M., AchutaRao, K., and Taylor, K. E.: Krakatoa's signature persists in the ocean, *Nature*, 429, 675, doi:10.1038/439675a, 2006.
- Goosse, H. and Renssen, H.: Regional response of the climate system to solar forcing: the role of the ocean, *Space Sci. Rev.*, 125, 227–235, doi:10.1007/s1124-006-9059-0, 2006.
- Goosse, H., Crowley, T., Zorita, E., Ammann, C., Renssen, H., and Driesschaert, E.: Modelling the climate of the last millen-

- nium: What causes the differences between simulations?, *Geophys. Res. Lett.*, 32, L06710, doi:10.1029/2005GL022368, 2005.
- Gray, L., Beer, J., Geller, M., Haigh, J. D., Lockwood, M., Matthes, K., Cubasch, U., Fleitmann, D., Harrison, G., Hood, L., Luterbacher, J., Meehl, G. A., Shindell, D., van Geel, B., and White, W.: Solar influenced on climate, *Rev. Geophys.*, 48, RG4001, doi:10.1029/2009RG000282, 2010.
- Gray, S., Graumlich, L. J., Betancourt, J. L., and Pederson, G. T.: A tree-ring based reconstruction of the Atlantic Multidecadal Oscillation since 1567 A.D., *J. Geophys. Res.*, 31, L12205, doi:10.1029/2004GL019932, 2004.
- Grinsted, A., Moore, J. C., and Jevrejeva, S.: Application of the cross wavelet transform and wavelet coherence to geophysical time series, *Nonlin. Processes Geophys.*, 11, 561–566, doi:10.5194/npg-11-561-2004, 2004.
- Hofer, D., Raible, C. C., and Stocker, T. F.: Variations of the Atlantic meridional overturning circulation in control and transient simulations of the last millennium, *Clim. Past*, 7, 133–150, doi:10.5194/cp-7-133-2011, 2011.
- Hourdin, F., Musat, I., Bony, S., Braconnot, P., Codron, F., Dufresne, J., Fairhead, L., Filiberti, M. A., Friedlingstein, P., Grandpeix, J. Y., Krinner, G., Levan, P., Li, Z., and Lott, F.: The LMDZ4 general circulation model: climate performance and sensitivity to parametrized physics with emphasis on tropical convection, *Clim. Dyn.*, 27, 787–813, doi:10.1007/s00382-006-0158-0, 2006.
- Jansen, E., Overpeck, J., Briffa, K. R., Duplessy, J.-C., Joos, F., Masson-Delmotte, V., Olago, B., Otto-Bliesner, B., Peliter, W. R., Rahmstorf, S., Ramesh, R., Raynaud, D., Rind, D., Solomina, O., Villalba, R., and Zhang, D.: Paleoclimate, in: *Climate change 2007: the physical science basis. Contribution of working group I to the fourth assessment report of the intergovernmental panel on climate change*, edited by: Solomon, S., Qin, S., Manning, M., Chen, Z., Marquis, M., Averyt, K. B., Tignor, M., and Miller, H. L., Cambridge University Press, 433–497, 2007.
- Jones, G. S., Gregory, J. M., Stott, P. A., Tett, S. F. B., and Thorpe, R. B.: An AOGCM simulation of the climate response to a volcanic super-eruption, *Clim. Dyn.*, 25, 725–738, doi:10.1007/s00382-005-0066-8, 2005.
- Jones, P. D., Osborn, T. J., and Briffa, K. R.: The evolution of climate over the last millennium, *Science*, 292, 662–667, doi:10.1126/science.1059126, 2001.
- Knight, J., Allan, R., Folland, C., Vellinga, M., and Mann, M.: A signature of persistent natural thermohaline circulation cycles in observed climate, *Geophys. Res. Lett.*, 32, L20708, doi:10.1029/2005GL024.233, 2005.
- Krinner, G., Viovy, N., de Noblet-Ducoudre, N., Ogee, J., Polcher, J., Friedlingstein, P., Ciais, P., Sitch, S., and Prentice, I. C.: A dynamic global vegetation for studies of the coupled atmosphere-biosphere system, *Glob. Biogeochem. Cy.*, 19, doi:10.1029/2003GB002199, 2005.
- Kuroda, Y., Yamazaki, K., and Shibata, K.: Role of ozone in the solar cycle modulation of the North Atlantic Oscillation, *J. Geophys. Res.*, 113, D14122, doi:10.1029/2007JD009336, 2008.
- Laurian, A., Lazar, A., and Reverdin, G.: Generation Mechanism of Spiciness Anomalies: An OGCM Analysis in the North Atlantic Subtropical Gyre, *J. Phys. Oceanogr.*, 39, 1003–1018, doi:10.1175/2008JPO3896.1, 2009.
- Madec, G., Delecluse, P., Imbard, M., and Levy, M.: OPA 8.1, ocean general circulation model reference manual, Notes du pole de modelisation, n. 11 Institut Pierre-Simon Laplace (IPSL), Paris, France, 1998.
- Mann, M., Zhang, Z., Rutherford, S., Bradley, R., Hughes, M., Shindell, D., Ammann, C., Faluguevi, G., and Ni, F.: Global Signatures and Dynamical Origins of the Little Ice Age and Medieval Climate Anomaly, *Science*, 326, 1256–1260, doi:10.1126/science.1177303, 2009.
- Marti, O., Braconnot, P., Dufresne, J. L., Bellier, J., Benschila, R., Bony, S., Brockmann, P., Cadule, P., Caubel, A., Codron, F., de Noblet, N., Denvil, S., Fairhead, L., Fichefet, T., Foujols, M. A., Friedlingstein, P., Goosse, H., Grandpeix, J. Y., Guilyardi, E., Hourdin, F., Krinner, G., Lvy, C., Madec, G., Mignot, J., Musat, I., Swingedouw, D., and Talandier, C.: Key features of the IPSL ocean atmosphere model and its sensitivity to atmospheric resolution, *Clim. Dyn.*, 34, 1–26, doi:10.1007/s00382-009-0640-6, 2010.
- Masse, G., Rowland, S. J., Sicre, M.-A., Jacob, J., Jansen, E., and Belt: Abrupt climate changes for Iceland during the last millennium: Evidence from high resolution sea ice reconstructions, *Earth Planet. Sc. Lett.*, 269, 564–568, doi:10.1016/j.epsl.2008.03.017, 2008.
- Meehl, G., Arblaster, J., Branstator, G., and van Loon, H.: A coupled air-sea response mechanism to solar forcing in the Pacific region, *J. Clim.*, 21, 2883–2897, doi:10.1175/2007JCLI1776.1, 2008.
- Meehl, G., Arblaster, J., Matthes, K., Sassi, F., and van Loon, H.: Amplifying the Pacific Climate System Response to a Small 11-Year Solar Cycle Forcing, *Science*, 325, 1114–1118, doi:10.1126/science.1172872, 2009.
- Mignot, J. and Frankignoul, C.: On the interannual variability of surface salinity in the Atlantic, *Clim. Dyn.*, 20, 555–565, doi:10.1007/s00382-002-0294-0, 2003.
- Mignot, J. and Frankignoul, C.: Interannual to interdecadal variability of sea surface salinity in the Atlantic and its link to the atmosphere in a coupled model, *J. Geophys. Res.*, 109, C04005, doi:10.1029/2003JC002005, 2004.
- Mignot, J. and Frankignoul, C.: On the variability of the Atlantic meridional overturning circulation, the North Atlantic Oscillation and the El Niño-Southern Oscillation in the Bergen Climate Model, *J. Clim.*, 18, 2361–2375, doi:10.1175/JCLI3405.1, 2005.
- Minnis, P., Harrison, E. F., Stowe, L. L., Gibson, G. G., Denn, F. M., Doelling, R., and Jr, Smith, W. L.: Radiative Climate Forcing by the Mount Pinatubo Eruption, *Science*, 259, 1411–1415, doi:10.1126/science.259.5100.1411, 1993.
- Msadek, R. and Frankignoul, C.: Variability of the meridional overturning circulation and its influence onto the atmosphere in the IPSL climate model, *Clim. Dyn.*, 33, 45–62, doi:10.1007/s00382-008-0452-0, 2009.
- Myneni, R. B., Nemani, R. R., and Running, S. W.: Estimation of global leaf area index and absorbed par using radiative transfer models, *Ieee T. Geosci. Remote.*, 35, 1380–1393, 1997.
- Oman, L.: High latitude eruption cast shadow over the african monsoon and the flow of the Nile, *Geophys. Res. Letters*, 33, L18711, doi:10.1029/2006GL027665, 2006.
- Ortega, P., Montoya, M., Gonzales-Rouco, F., Mignot, J., and Legutke, S.: Variability of the Atlantic meridional overturning circulation in the last millennium and two IPCC scenarios, *Clim.*

- Dyn., in press, 2011.
- Ottera, O. H., Bentsen, M., Drange, H., and Suo, L.: External forcing as a metronome for Atlantic multidecadal variability, *Nature Geoscience*, 3, 688–694, doi:10.1038/ngeo955, 2010.
- Richter, T. O., Peeters, F., and van Weering, T.: Late Holocene (0–2.4 ka BP) surface water temperature and salinity variability, Feni Drift, NE Atlantic Ocean, *Quaternary Sci. Rev.*, 28, 1941–1955, doi:10.1016/j.quascirev.2009.04.008, 2009.
- Robock, A.: Volcanic eruptions and climate, *Rev. Geophys.*, 38, 191–219, doi:10.1029/1998RG000054, 2000.
- Robock, A. and Mao, J.: Winter warming from large volcanic eruptions, *Geophys. Res. Lett.*, 19, 2405–2408, doi:10.1029/92GL02627, 1992.
- Schmidt, G. A., Jungclaus, J. H., Ammann, C. M., Bard, E., Braconnot, P., Crowley, T. J., Delaygue, G., Joos, F., Krivova, N. A., Muscheler, R., Otto-Bliesner, B. L., Pongratz, J., Shindell, D. T., Solanki, S. K., Steinhilber, F., and Vieira, L. E. A.: Climate forcing reconstructions for use in PMIP simulations of the last millennium (v1.0), *Geosci. Model Dev.*, 4, 33–45, doi:10.5194/gmd-4-33-2011, 2011.
- Schneider, D. P., Ammann, C. M., Otto-Bliesner, B. L., and Kaufman, D. S.: Climate response to large, high latitude and low-latitude volcanic eruptions in the Community Climate System Model, *J. Geophys. Res.*, 114, D05101, doi:10.1029/2008JD011222, 2009.
- Servonnat, J., Yiou, P., Khodri, M., Swingedouw, D., and Denvil, S.: Influence of solar variability, CO₂ and orbital forcing between 1000 and 1850 AD in the IPSLCM4 model, *Clim. Past*, 6, 445–460, doi:10.5194/cp-6-445-2010, 2010.
- Shapiro, A., Schmutz, W., Rozanov, E., Schoell, M., Haberleiter, M., Shapiro, A. V., and Nyeki, S.: A new approach to the long-term reconstruction of the solar irradiance leads to large historical solar forcing, *Astronomy and Astrophysics*, 529, 16173 pp., 2011.
- Shindell, D., Schmidt, G. A., Miller, R. L., and Mann, M. E.: Volcanic and solar forcing of climate change during the preindustrial era, *J. Clim.*, 16, 4094–4107, doi:10.1175/1520-0442, 2003.
- Shindell, D., Schmidt, G. A., Mann, M. E., and Faluvegi, G.: Dynamic winter climate response to large tropical volcanic eruptions since 1600, *J. Geophys. Res.*, 109, D05104, doi:10.1029/2003JD004151, 2004.
- Sicre, M., Jacob, J., Ezat, U., Rousse, S., Kissel, C., Yiou, P., Eriksson, J., Knudsen, K. L., Jansen, E., and Turon, J. L.: Decadal variability of sea surface temperatures off North Iceland over the last 2000 years, *EPSL*, 268, 137–142, doi:10.1016/j.epsl.2008.01.011, 2008.
- Sicre, M., Hall, I., Mignot, J., Khodri, M., Ezat, U., Truong, M.-X., Eriksson, J. J., and Knudsen, K. L.: Sea surface temperature variability in the subpolar Atlantic over the last two millennia, *Paleoc.*, in press, 2011.
- Solanki, S. K. and Krivova, N. A.: Solar variability of possible relevance for planetary climates, *Space Sci. Rev.*, 125, 25–37, doi:10.1007/s11214-006-9044-7, 2006.
- Stenchikov, G., Hamilton, K., Stouffer, R., Robock, A., Ramaswamy, V., Santer, B., and Graf, H.-F.: Arctic Oscillation response to volcanic eruptions in the IPCC AR4 climate models, *J. Geophys. Res.*, 111, D07107, doi:10.1029/2005JD006286, 2004.
- Stenchikov, G., Delworth, T. L., Ramaswamy, V., Stouffer, R. J., Wittenberg, A., and Zeng, F.: Volcanic signals in oceans, *J. Geophys. Res.*, 114, D16104, doi:10.1029/2008JD011673, 2009.
- Stendel, M., Mogensen, I., and Christensen, J.: Influence of various forcings on global climate in historical times using a coupled atmosphere-ocean general circulation model, *Clim. Dynam.*, 26, 1–15, doi:10.1007/s00382-005-0041-4, 2006.
- Sutton, R. T. and Hodson, D. L. R.: Influence of the Ocean on North Atlantic Climate Variability: 1871–1999, *J. Clim.*, 16, 3296–3313, doi:10.1175/1520-0442, 2003.
- Sutton, R. T. and Hodson, D. L. R.: Atlantic Ocean Forcing of North American and European Summer Climate, *Science*, 309, 5731, 115–118, doi:10.1126/science.110949616, 2005.
- Swingedouw, D., Braconnot, P., Delecluse, P., Guilyardi, E., and Marti, O.: The impact of global freshwater forcing on the thermohaline circulation: adjustment of North Atlantic convection sites in a CGCM, *Clim. Dyn.*, 28, 291–305, doi:10.1007/s00382-006-0171-3, 2007.
- Timmreck, C., Lorenz, S. J., Crowley, T. J., Kinne, S., Raddatz, T. J., Thomas, M. A., and Jungclaus, J. H.: Limited temperature response to the very large AD 1258 volcanic eruption, *Geophys. Res. Letters*, 36, L21708, doi:10.1029/2009GL040083, 2009.
- Torrence, C. and Compo, G. P.: A practical guide to wavelet analysis, *Bull. Am. Meteorol. Soc.*, 9, 61–78, 1998.
- Trenberth, K. and Dai, A.: Effect of Mount Pinatubo volcanic eruption on the hydrological cycle as analog of geoengineering, *Geophys. Res. Letters*, 34, L15702, doi:10.1029/2007GL030524, 2007.
- Valcke, S., Terray, L., and Piacentini, A.: Oasis 2.4, Ocean atmosphere sea ice soil: user's guide, Tech. Rep. TR/CMGC/00/10, CERFACS, Toulouse, France, 2000.
- van der Schrier, G., Weber, S., and Drijfhout, S. S.: Sea level changes in the North Atlantic by solar forcing and internal variability, *Clim. Dyn.*, 19, 435–447, doi:10.1007/s00382-002-0235-y, 2002.
- Vieira, L. and Solanki, S.: Evolution of the solar magnetic flux on time scales of years to millennia, *Annu. Rev. Astron. Astr.*, 509, arXiv/0911.4396, doi:10.1051/00046361/200913276, 2009.
- Zanchettin, D., Timmreck, C., Graf, H.-F., Rubino, A., Lorenz, S., Lohmann, K., Kruger, K., and Jungclaus, J. H.: Bi-decadal variability excited in the coupled ocean-atmosphere system by strong tropical volcanic eruptions, *Clim. Dyn.*, in press, doi:10.1007/s00382-011-1167-1, 2011.
- Zhong, Y., Miller, G. H., Otto-Bliesner, B. L., Holland, M. M., Bailey, D. A., Schneider, D. P., and Geirsdottir, A.: Centennial-scale climate change from decadal-paced explosive volcanism: a coupled sea ice-ocean mechanism, *Clim. Dyn.*, 37, 2373–2387, doi:10.1007/s00382-010-0967-z, 2011.
- Zorita, E., von Storch, H., Gonzales-Rouco, F., Cubasch, U., Luterbacher, J., Legutke, S., Fischer-Bruns, I., and Schlese, U.: Climate evolution in the last five centuries simulated by an ocean-atmosphere model: global temperatures, the North Atlantic Oscillation and the Late Maunder Minimum, *Meteorol. Z.*, 13, 271–289, doi:10.1127/0941-2894/2004/0013-0271, 2004.